PHYSICAL REVIEW B **94**, 041103(R) (2016)

Resistivity plateau and extremely large magnetoresistance in $NbAs_2$ and $TaAs_2$

Yi-Yan Wang, Qiao-He Yu, Peng-Jie Guo, Kai Liu, and Tian-Long Xia*

Department of Physics, Beijing Key Laboratory of Opto-electronic Functional Materials & Micro-nano Devices, Renmin University of China, Beijing 100872, People's Republic of China

(Received 8 March 2016; revised manuscript received 13 June 2016; published 5 July 2016)

In topological insulators (TIs), metallic surface conductance saturates the insulating bulk resistance with decreasing temperature, resulting in resistivity plateau at low temperatures as a transport signature originating from metallic surface modes protected by time reversal symmetry (TRS). Such a characteristic has been found in several materials including Bi_2Te_2Se, SmB_6 etc. Recently, similar behavior has been observed in metallic compound LaSb, accompanying an extremely large magnetoresistance (XMR). Shubnikov-de Hass (SdH) oscillation at low temperatures further confirms the metallic behavior of the plateau region under magnetic fields. LaSb [Tafti *et al.*, Nat. Phys. **12**, 272 (2015)] has been proposed by the authors as a possible topological semimetal (TSM), while negative magnetoresistance is absent at this moment. Here, high quality single crystals of $NbAs_2$/$TaAs_2$ with inversion symmetry have been grown, and the resistivity under magnetic field is systematically investigated. Both of them exhibit metallic behavior under zero magnetic field, and a metal-to-insulator transition occurs when a nonzero magnetic field is applied, resulting in XMR (1.0×10^5% for $NbAs_2$ and 7.3×10^5% for $TaAs_2$ at 2.5 K and 14 T). With temperature decreased, a resistivity plateau emerges after the insulatorlike regime, and SdH oscillation has also been observed in $NbAs_2$ and $TaAs_2$.

DOI: 10.1103/PhysRevB.94.041103

I. INTRODUCTION

The magnetoresistance (MR) of materials is an interesting research topic in the condensed matter community [1]. Since the discovery of giant magnetoresistance (GMR) in magnetic multilayer [2,3] and colossal magnetoresistance (CMR) in magnetic oxide materials [4,5], people have always been looking for materials with higher MR. In general, nonmagnetic metals only have small MR. Recently, XMR of about 10^5%–10^6% has been observed in several nonmagnetic metals, such as TX (T=Ta/Nb, X=As/P) [6–14], $NbSb_2$ [15], LaSb [1], Cd_3As_2 [16–19], and WTe_2 [20–23] etc. In these materials, TX is an important system which is composed of VB elements and pnicogen, all of which are proved to be Weyl semimetals [24–34]. Extraordinary properties such as Fermi arc and chiral anomaly observed in TX have attracted great attention. Considering previous research on $NbSb_2$ [15], which shows XMR and possible Dirac points, despite that TX_2 type compounds have a monoclinic structure without broken inversion symmetry which results in the appearance of Weyl nodes in TX, topological characteristic is also possible in TX_2 compounds. Searching for more members of TX_2 materials will be helpful to understand this system. In this Rapid Communication, we focus on the TX_2 type arsenides.

In addition to XMR, the field induced resistivity plateau is also an interesting phenomenon. The plateau is a universal behavior in topological insulators [35,36], which originates from the metallic surface conductance saturating the insulating bulk resistance [1]. TRS protects the metallic surface state and is indispensable in TIs. Recent research in possible TSM candidate LaSb shows that there also exists a plateau when TRS is broken [1]. Although the specific mechanism of this feature is still a mystery, it is meaningful to find out more materials with such a property.

In this Rapid Communication, we have mainly studied the resistivity and magnetoresistance of two synthesized single crystalline compounds: $NbAs_2$ and $TaAs_2$. Metal-to-insulator transition and XMR arise at low temperature and high field. The observed resistivity plateau is similar to the universal behavior in TIs, in which TRS is preserved, while TRS is broken in our measurements as the case in LaSb. Analysis of SdH effect observed in $NbAs_2$ and $TaAs_2$ implies the complex Fermi surface structure, and the two major oscillation frequencies reveal there may exist two Fermi pockets in each of the samples. Band structure calculations show the existence of several electronlike and holelike Fermi surfaces with different sizes in $NbAs_2$/$TaAs_2$.

II. EXPERIMENTAL AND CRYSTAL STRUCTURE

High-quality single crystals of $NbAs_2$ and $TaAs_2$ were obtained by chemical vapor transport method. Firstly, polycrystal of these two compounds was prepared by solid state reaction. The mixtures of Nb/Ta powder and As powder were sealed in a quartz tube with a ratio of 1:2. For $NbAs_2$, the tube furnace was heated to 800 °C and held for 30 h; for $TaAs_2$ the tube furnace was heated to 750 °C. Secondly, 5 mg/cm^3 of iodine was used as transport agent to grow single crystals, and the temperature gradient was set as 1050 °C–850 °C. All the obtained crystals grow more easily along the *b* axis and form rodlike crystals. The atomic proportions determined by energy dispersive x-ray spectroscopy (EDS, Oxford X-Max 50) were consistent with 1:2 for (Nb/Ta):As. X-ray diffraction (XRD) patterns were obtained from powder of single crystals on a Bruker D8 Advance x-ray diffractometer using Cu K_α radiation. TOPAS-4.2 was employed for the refinements. Resistivity measurements were performed on a Quantum Design physical property measurement system (QD PPMS-14T).

The electronic structures of $NbAs_2$ and $TaAs_2$ have been studied by using the first-principles calculations. The projector augmented wave (PAW) method [37,38] as implemented in the

*tlxia@ruc.edu.cn

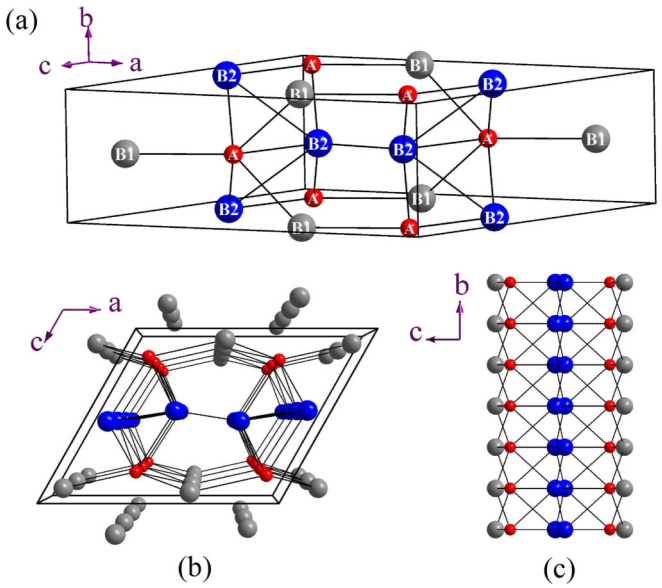

FIG. 1. Crystal structure of $NbAs_2$ and $TaAs_2$. (a) Unit cell of the crystal. A represents Nb or Ta atoms, B1 and B2 represent type-I and type-II atoms of As, respectively. (b),(c) Views of the structure from *b*-axis and *a*-axis directions, respectively.

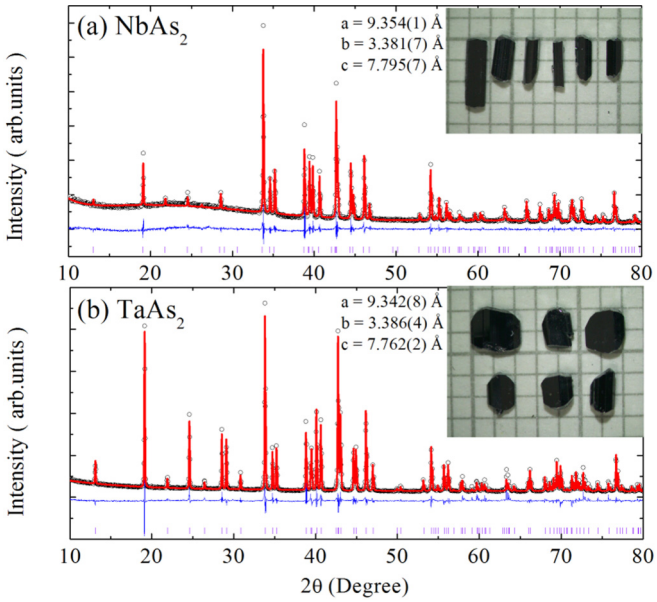

FIG. 2. XRD patterns of $NbAs_2$ and $TaAs_2$ with refinement. Observed curves are in black circles and the calculated curves are in red lines. The difference curve is in blue and the violet vertical lines denote the positions of Bragg reflections of $NbAs_2$ and $TaAs_2$ with PDF No. 01-086-0520 and No. 01-089-3409. Refined lattice parameters are shown in each picture. $R_{wp} = 6.69\%$, 8.73% for $NbAs_2$ and $TaAs_2$. Insets show the grown crystals.

VASP package [39–41] was used to describe the core electrons. For the exchange-correlation potential, two different levels (the GGA and meta-GGA) in the Jacob's ladder [42] were adopted. In the GGA level, the Perdew-Burke-Ernzerhof (PBE) formula [43] was employed, while in the meta-GGA level, the modified Becke-Johnson (MBJ) [44,45] exchange potential with the GGA correlation was used. The kinetic energy cutoff of the plane-wave basis was set to be 300 eV. A $15\times15\times10$ *k*-point mesh was utilized for the Brillouin zone (BZ) sampling, and the Fermi surface was broadened by the Gaussian smearing method with a width of 0.05 eV. Both cell parameters and internal atomic positions were allowed to relax until all forces were smaller than 0.01 eV/Å. Once the equilibrium crystal structures were obtained, the electronic structures were calculated by including the spin orbital coupling (SOC) effect. The Fermi surface were studied by using the maximally localized Wannier functions (MLWF) [46,47].

$NbAs_2$ and $TaAs_2$ crystallize in a complex structure [48,49]. Figure 1 shows the structure of these compounds from different views. In the structure, there is one type of Nb/Ta atoms denoted as A and two types of As atoms denoted as B1 or B2. Each A is surrounded by six B, including three B1 and three B2. Each B2 is coordinated to three other B2. In these crystals, the *b* axis is the easy growth axis, and this characteristic can be seen clearly from the *a*-axis direction as shown in Fig. 1(c). Figures 2(a) and 2(b) show powder x-ray diffraction patterns and refinements of $NbAs_2$ and $TaAs_2$ crystals. The reflections are well indexed in space group $C_{12/m1}$. The refined lattice parameters are given in the figures, consistent with previously reported results [48–50].

III. RESULTS AND DISCUSSIONS

Figures 3(a) and 3(d) plot the temperature dependence of resistivity under different magnetic fields. The electric current is parallel to the *b* axis, and the magnetic field is parallel to the *ac* plane. For both compounds, the temperature dependent resistivity at zero field exhibits a metallic behavior. The high residual resistivity ratio (RRR = 75, 83 for $NbAs_2$ and $TaAs_2$, respectively) indicates high quality of the samples. Extremely large MR has been observed in both of them. At 2.5 K and 14 T, MR = $1.0\times10^5\%$ and $7.3\times10^5\%$ for $NbAs_2$ and $TaAs_2$, respectively. With temperature reduced, a magnetic field-induced metal-to-insulator-like transition is observed. An interesting feature is that a resistivity plateau appears instead of the resistivity continuing to increase with further decreasing temperature. Temperatures of the resistivity plateau appearing are about 28 K and 19 K for $NbAs_2$ and $TaAs_2$, respectively. At high field, the plateau becomes distorted because of the effect of SdH oscillation, which will be discussed later. In general, topological insulators have an insulating bulk state and a metallic surface state. The TRS protects the metallic surface state in topological insulators. Along with the appearance of the metallic surface conduction, the insulating resistivity will reach saturation resulting in a resistivity plateau. In our situation, the existence of magnetic field breaks the TRS, but there is still a plateau at low temperature. Such properties have been observed in TX [7–14], $NbSb_2$ [15], and WTe_2 [20–23], where the properties are attributed to field induced metal-insulator transition or Kohler's rule in high quality samples with low charge carrier density.

Plots of $d\rho/dT$ against temperature are displayed in Figs. 3(b) and 3(e). The temperature of metal-to-insulator transition is determined as T_1 where the value of $d\rho/dT$ becomes negative. From the figure, it can be judged that T_1 increases with the field. The starting temperature of the

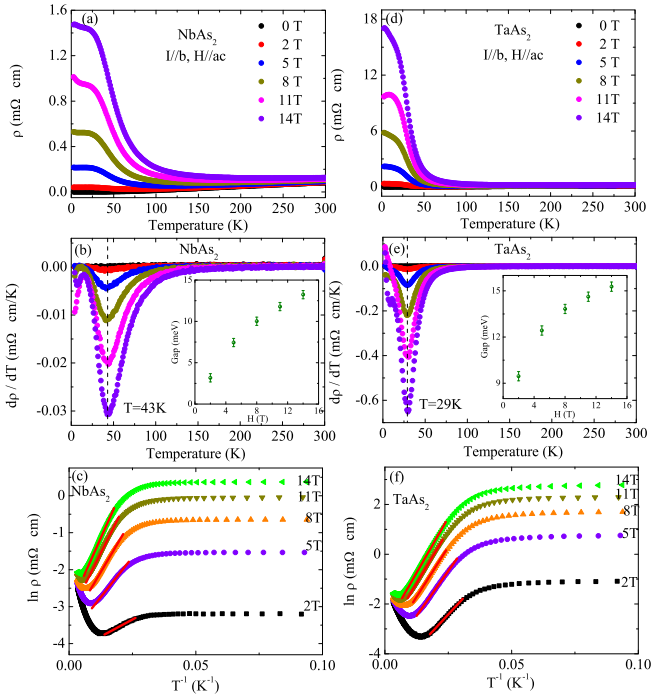

FIG. 3. (a), (d) Resistivity of $NbAs_2$ and $TaAs_2$ plotted as a function of temperature under different magnetic field (H=0, 2, 5, 8, 11, 14 T). I is parallel to the b axis and H is parallel to the ac plane. The metal-to-insulator-like transition and resistivity plateau are observed clearly. (b), (e) $d\rho/dT$ versus temperature for corresponding samples. The insets show the energy gap of the insulatorlike area. (c),(f) Plots of $\ln\rho$ against the reciprocal of temperature $1/T$. The values of energy gap are obtained by fitting the insulatorlike regions (the linear part in figures) using the relation $\rho(T) \propto \exp(\xi/k_BT)$. The red lines indicate the regions used in fittings.

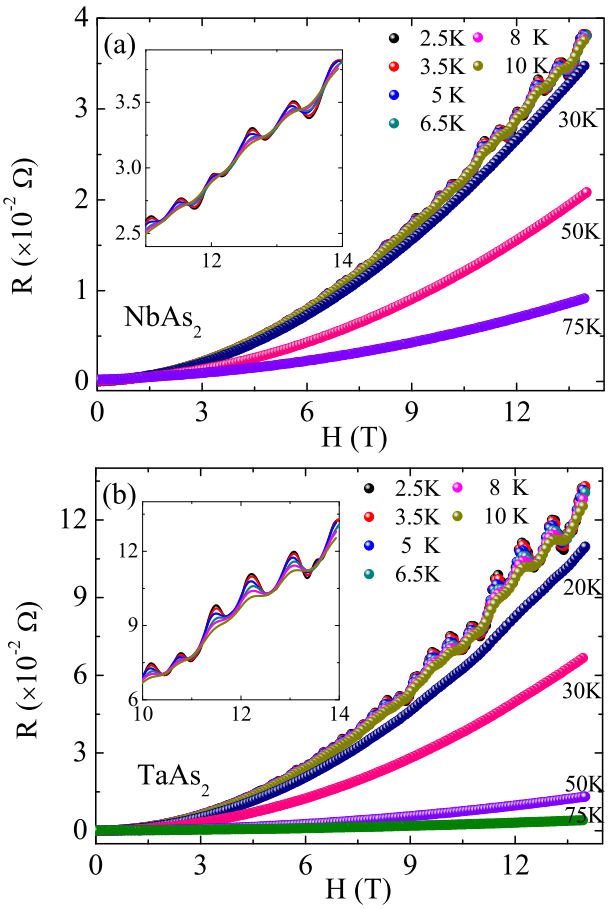

FIG. 4. Magnetic field dependence of resistance of $NbAs_2$ (a) and $TaAs_2$ (b) from 2.5 K to 75 K. The insets show the enlarged part of R-H from 10–14 T, where the oscillation can be observed more clearly.

resistivity plateau (T_2) can be defined as the temperature at the minimum of $d\rho/dT$. As shown in the figure, T_2 remains unchanged with the increase of magnetic field. T_1 increases but T_2 keeps unchanged, which suggests that the range of the insulatorlike area becomes larger along with increasing field, meanwhile the range of the resistivity plateau keeps invariant. The energy gaps are shown in the inset of Figs. 5(b) and 5(e). All the gap values are obtained through fitting the linear part in Figs. 3(c) and 3(f). At the magnetic field of $H = 14$ T, the energy gaps are 13.2 meV and 15.3 meV for $NbAs_2$ and $TaAs_2$, respectively. As a whole, $TaAs_2$ has the larger gap than $NbAs_2$.

Figures 4(a) and 4(b) show the resistance of $NbAs_2$ and $TaAs_2$ as a function of field. Clear SdH oscillation was observed at low temperature and high field. The insets show the enlarged images of the oscillating part. In both compounds, the MR-H curves (not shown here) all exhibit a semiclassical quadratic behavior ($MR \propto H^2$) [51]. With the increase of temperature, the MR becomes smaller and the oscillation gradually disappears.

Figures 5(a) and 5(b) plot the oscillation amplitude $\Delta R_{xx} = R_{xx} - \langle R_{xx}\rangle$ of $NbAs_2$ and $TaAs_2$ against the reciprocal of magnetic field 1/H at various temperatures. The amplitude displays a complex periodic behavior and decreases with increasing temperature. There are several peaks in the fast Fourier transformation (FFT) spectra [Figs. 5(c) and 5(d)], but the major peaks are α and β. The complexity of periodic behavior can be attributed to the effect of small peaks in the FFT spectra. For $NbAs_2$, the major oscillation frequencies are $F_\alpha = 90$ T and $F_\beta = 204$ T. For $TaAs_2$, $F_\alpha = 45$ T and $F_\beta = 158$ T. In SdH oscillation, the frequency F is proportional to the cross sectional area A of the Fermi surface normal to the magnetic field and can be described using Onsager relation $F = (\phi_0/2\pi^2)A = (\hbar/2\pi e)A$ [52]. Two major peaks in FFT spectra imply there are two major Fermi pockets in $NbAs_2$ and $TaAs_2$, which is similar to the situation in $NbSb_2$ [15]. In Figs. 5(e)–5(h), we display the temperature dependence of the relative FFT amplitude of frequencies α and β of $NbAs_2$ and $TaAs_2$, respectively. The thermal factor $R_T = (\lambda T)/\sinh(\lambda T)$ in Lifshitz-Kosevitch formula [52] has been employed to describe the temperature dependence of FFT amplitude Δ. In the formula, $\lambda = (2\pi^2 k_B m^*)/(\hbar e\bar{H})$, so the cyclotron effective mass m^* can be obtained from the fitting result. All the data can be fitted well and yields the effective mass. For $NbAs_2$, $m^*_\alpha = 0.20m_e$ and $m^*_\beta = 0.27m_e$; for $TaAs_2$, $m^*_\alpha = 0.17m_e$ and $m^*_\beta = 0.24m_e$. The insets of (e)–(h) show $1/H$ as a function of Landau level index n for corresponding oscillation frequencies. We assign integer indices to the ΔR_{xx} peak positions in $1/H$ and half integer indices to the

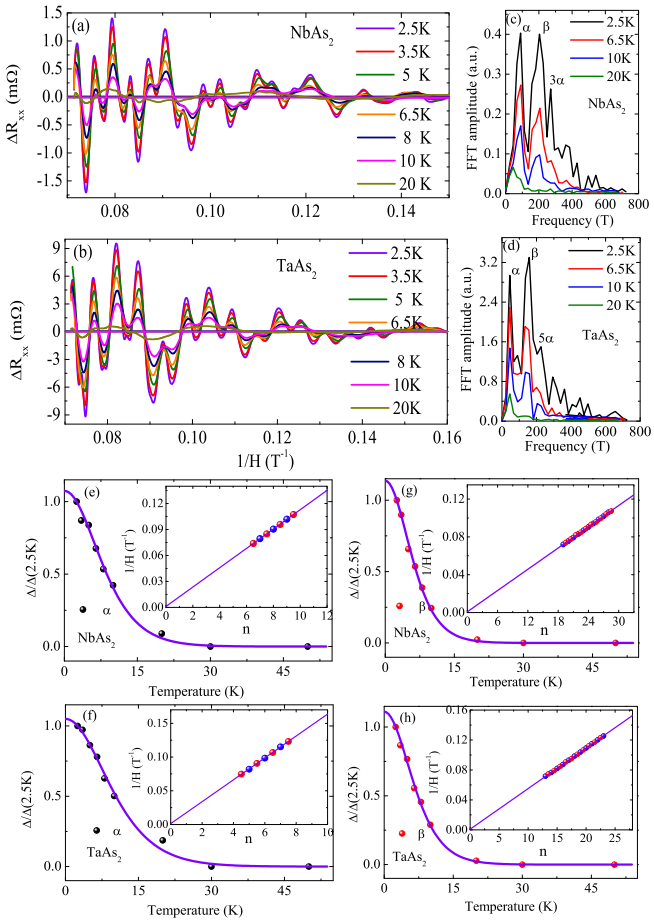

FIG. 5. Analyses of oscillations in $NbAs_2$ and $TaAs_2$. (a), (b) The amplitude of SdH oscillations plotted as a function of the reciprocal of magnetic field. (c), (d) The FFT spectra of the corresponding SdH oscillations at 2.5 K, 6.5 K, 10 K, and 20 K for $NbAs_2$ and $TaAs_2$. (e), (f) Temperature dependence of the relative FFT amplitude of oscillation frequency α. The violet solid lines are the fitting results based on Lifshitz-Kosevitch formula, which yields the effective cyclotron resonant mass. (g), (h) The same processing of oscillation frequency β. Insets: Landau index n plotted against $1/H$ for corresponding oscillation frequencies. The peaks (blue circles) and valleys (red circles) of the ΔR_{xx} at 2.5 K are assigned as integer and half integer LL indices, respectively.

ΔR_{xx} valley positions. The Landau index n is dependent on $1/H$ linearly according to Lifshitz-Onsager quantization rule $A(\hbar/2\pi eH) = n + 1/2 + \beta + \delta$. $2\pi\beta$ is the Berry phase. δ is a phase shift with the value of $\delta = 0$ (or $\pm 1/8$) for a 2D (or 3D) system. Nonzero Berry phase is a fundamental transport property associated with topological characteristic. The data points in the insets fall into a straight line. The intercepts obtained from linear extrapolation are close to zero, indicating the nontrivial Berry phases for corresponding bands. The nontrivial Berry phases reflect the topological characteristic of Fermi surfaces. ARPES experiments are needed to obtain more information about the Fermi surface, and the collaborative work based on our samples is already in process [53].

Figures 6(a) and 6(b) show the Hall effect data of $NbAs_2$ and $TaAs_2$. Clear oscillation also can be observed at low temperature and high field. The Hall resistivity ρ_{xy} is nonlinear

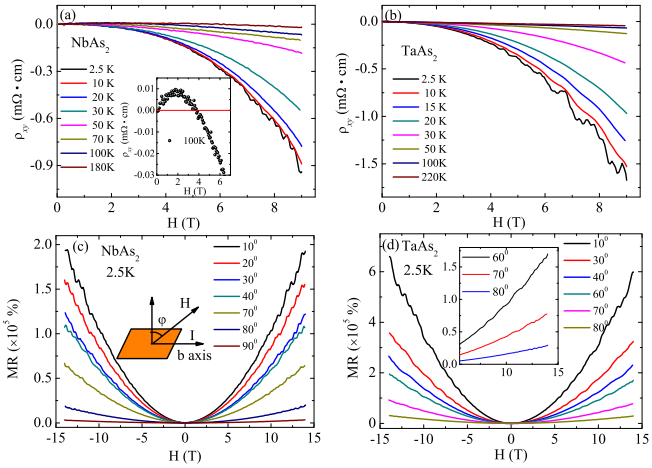

FIG. 6. (a), (b) Hall resistivity of $NbAs_2$ and $TaAs_2$ at various temperatures. The inset in (a) shows a typical sign change of Hall resistivity observed in $NbAs_2$. (c), (d) Field-dependent MR of $NbAs_2$ and $TaAs_2$ with different angles φ at $T = 2.5$ K. The definition of φ is shown in the inset of (c). The inset in (d) shows the enlarged image of (d) at larger angles.

for both of them, which indicates two types of carriers. The carrier mobilities are on the order of 10^5 cm^2 V^{-1} s^{-1} for both $NbAs_2$ and $TaAs_2$ at 2.5 K. As shown in the inset in (a), the change of sign from positive to negative occurs in $NbAs_2$, but the behavior has not been observed in $TaAs_2$. In Figs. 6(c) and 6(d), we present the field-dependent MR of $NbAs_2$ and $TaAs_2$ at 2.5 K and various φ. The electrical current **I** is always along the b axis direction, and the magnetic field **H** is tilted in different directions. With the direction of the magnetic field near the current direction, the MR decreases gradually and the oscillation still exists. These features imply the dominant 3D anisotropic Fermi surface in $NbAs_2$ and $TaAs_2$.

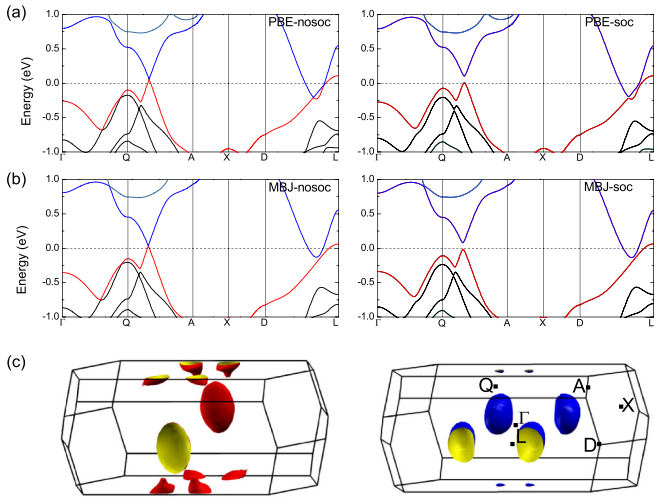

FIG. 7. Band structures of $NbAs_2$ calculated with (a) the PBE functional and (b) MBJ exchange potential. The "soc" denotes the spin-orbital coupling (SOC) effect and the "nosoc" without the SOC effect. (c) The corresponding Fermi surface of $NbAs_2$ calculated with the PBE functional and including the SOC effect.

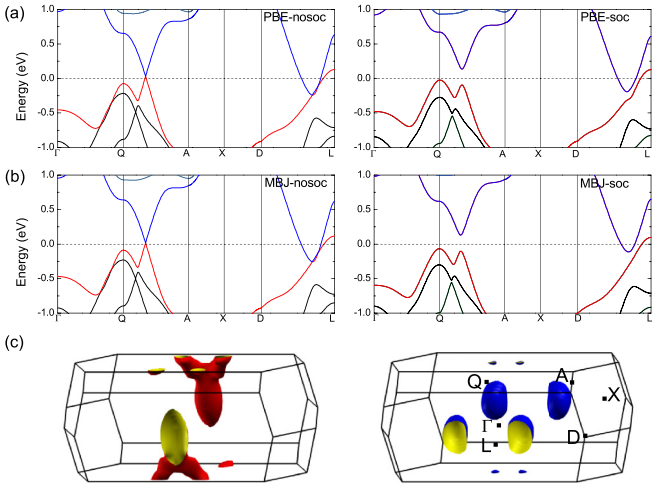

FIG. 8. Band structures of $TaAs_2$ calculated with (a) the PBE functional and (b) MBJ exchange potential. The "soc" denotes the spin-orbital coupling (SOC) effect and the "nosoc" without the SOC effect. (c) The corresponding Fermi surface of $TaAs_2$ calculated with the PBE functional and including the SOC effect.

The electronic structures of $NbAs_2/TaAs_2$ have also been studied from first-principles calculations. Since $NbAs_2/TaAs_2$ are semimetals, their band structures along high symmetry directions of Brillouin zone (BZ) have been calculated by using both the PBE functional and the MBJ potential. As shown in Figs. 7 and 8, the band structure and Fermi surface of $NbAs_2$ and $TaAs_2$ are very close to each other. A band gap opens along the Q-A direction only when the SOC effect is included. Comparing the PBE results in panel (a) with the MBJ results in panel (b) of both Figs. 7 and 8, minor changes can be discerned, demonstrating that the PBE functional in the GGA level is able to describe the electronic structures well here. The Fermi surface of $NbAs_2$ and $TaAs_2$ calculated with the PBE functional and including the SOC effect are shown in Figs. 7(c) and 8(c), respectively. The color sets of these Fermi surfaces are in a one-to-one relationship with the corresponding bands crossing the Fermi level along the D-L direction. Both of them have several hole pockets coexisting with a few pairs of electron pockets, suggesting the feature of multiple Fermi surfaces.

IV. SUMMARY

In summary, single crystals of $NbAs_2$ and $TaAs_2$ have been grown successfully. Resistivity has been measured and magnetoresistance has been analyzed in detail. Field-induced metal-to-insulator transition and XMR are observed in both samples. The resistivity plateau similar to topological insulator emerges after the insulatorlike regime, which is similar to previous work on the LaSb crystal. Moreover, with the increase of field, clear SdH oscillation is observed in $NbAs_2$ and $TaAs_2$. The FFT spectra reveal there exist two major frequencies in the oscillation and the corresponding effective mass are obtained. Electronic structure calculation shows the coexistence of several electronlike and holelike Fermi surfaces in $NbAs_2/TaAs_2$. As possible candidates of TSM, related ARPES studies on $NbAs_2$ and $TaAs_2$ are expected.

Note added. Recently, one related work on $TaSb_2$ is reported online [54], where resistivity plateau, XMR, SdH oscillation, and negative MR have been observed by the authors.

ACKNOWLEDGMENTS

This work is supported by the National Natural Science Foundation of China (No. 11574391), the Fundamental Research Funds for the Central Universities, and the Research Funds of Renmin University of China (No. 14XNLQ03 and 14XNLQ07). Computational resources have been provided by the Physical Laboratory of High Performance Computing at RUC. The Fermi surfaces were prepared with the XCRYSDEN program [55].

[1] F. Tafti, Q. Gibson, S. Kushwaha, N. Haldolaarachchige, and R. Cava, Nat. Phys. **12**, 272 (2015).

[2] M. N. Baibich, J. M. Broto, A. Fert, F. N. Van Dau, F. Petroff, P. Etienne, G. Creuzet, A. Friederich, and J. Chazelas, Phys. Rev. Lett. **61**, 2472 (1988).

[3] G. Binasch, P. Grünberg, F. Saurenbach, and W. Zinn, Phys. Rev. B **39**, 4828 (1989).

[4] Y. Moritomo, A. Asamitsu, H. Kuwahara, and Y. Tokura, Nature (London) **380**, 141 (1996).

[5] A. Ramirez, J. Phys.: Condens. Matter **9**, 8171 (1997).

[6] H. Weng, C. Fang, Z. Fang, B. A. Bernevig, and X. Dai, Phys. Rev. X **5**, 011029 (2015).

[7] X. Huang, L. Zhao, Y. Long, P. Wang, D. Chen, Z. Yang, H. Liang, M. Xue, H. Weng, Z. Fang *et al.*, Phys. Rev. X **5**, 031023 (2015).

[8] N. J. Ghimire, Y. Luo, M. Neupane, D. J. Williams, E. D. Bauer, and F. Ronning, J. Phys.: Condens. Matter **27**, 152201 (2015).

[9] X. Yang, Y. Liu, Z. Wang, Y. Zheng, and Z.-A. Xu, arXiv:1506.03190.

[10] F. Arnold, C. Shekhar, S.-C. Wu, Y. Sun, M. Schmidt, N. Kumar, A. G. Grushin, J. H. Bardarson, R. D. d. Reis, M. Naumann *et al.*, Nat. Commun. **7**, 11615 (2016).

[11] J. Hu, J. Liu, D. Graf, S. Radmanesh, D. Adams, A. Chuang, Y. Wang, I. Chiorescu, J. Wei, L. Spinu *et al.*, Sci. Rep. **6**, 18674 (2015).

[12] C. Zhang, C. Guo, H. Lu, X. Zhang, Z. Yuan, Z. Lin, J. Wang, and S. Jia, Phys. Rev. B **92**, 041203 (2015).

[13] C. Shekhar, A. K. Nayak, Y. Sun, M. Schmidt, M. Nicklas, I. Leermakers, U. Zeitler, Y. Skourski, J. Wosnitza, and Z. Liu, Nat. Phys. **11**, 645 (2015).

[14] Z. Wang, Y. Zheng, Z. Shen, Y. Zhou, X. Yang, Y. Li, C. Feng, and Z.-A. Xu, Phys. Rev. B **93**, 121112(R) (2016).

[15] K. Wang, D. Graf, L. Li, L. Wang, and C. Petrovic, Sci. Rep. **4**, 7328 (2014).

[16] M. Neupane, S.-Y. Xu, R. Sankar, N. Alidoust, G. Bian, C. Liu, I. Belopolski, T.-R. Chang, H.-T. Jeng, H. Lin *et al.*, Nat. Commun. **5**, 3786 (2014).

[17] S. Borisenko, Q. Gibson, D. Evtushinsky, V. Zabolotnyy, B. Büchner, and R. J. Cava, Phys. Rev. Lett. **113**, 027603 (2014).
[18] T. Liang, Q. Gibson, M. N. Ali, M. Liu, R. Cava, and N. Ong, Nat. Mater. **14**, 280 (2015).
[19] L. P. He, X. C. Hong, J. K. Dong, J. Pan, Z. Zhang, J. Zhang, and S. Y. Li, Phys. Rev. Lett. **113**, 246402 (2014).
[20] M. N. Ali, J. Xiong, S. Flynn, J. Tao, Q. D. Gibson, L. M. Schoop, T. Liang, N. Haldolaarachchige, M. Hirschberger, N. P. Ong *et al.*, Nature (London) **514**, 205 (2014).
[21] Z. Zhu, X. Lin, J. Liu, B. Fauqué, Q. Tao, C. Yang, Y. Shi, and K. Behnia, Phys. Rev. Lett. **114**, 176601 (2015).
[22] L. R. Thoutam, Y. L. Wang, Z. L. Xiao, S. Das, A. Luican-Mayer, R. Divan, G. W. Crabtree, and W. K. Kwok, Phys. Rev. Lett. **115**, 046602 (2015).
[23] Y. L. Wang, L. R. Thoutam, Z. L. Xiao, J. Hu, S. Das, Z. Q. Mao, J. Wei, R. Divan, A. Luican-Mayer, G. W. Crabtree *et al.*, Phys. Rev. B **92**, 180402 (2015).
[24] S.-Y. Xu, I. Belopolski, N. Alidoust, M. Neupane, G. Bian, C. Zhang, R. Sankar, G. Chang, Z. Yuan, C.-C. Lee *et al.*, Science **349**, 613 (2015).
[25] S.-M. Huang, S.-Y. Xu, I. Belopolski, C.-C. Lee, G. Chang, B. Wang, N. Alidoust, G. Bian, M. Neupane, C. Zhang *et al.*, Nat. Commun. **6**, 7373 (2015).
[26] B. Q. Lv, H. M. Weng, B. B. Fu, X. P. Wang, H. Miao, J. Ma, P. Richard, X. C. Huang, L. X. Zhao, G. F. Chen *et al.*, Phys. Rev. X **5**, 031013 (2015).
[27] B. Lv, N. Xu, H. Weng, J. Ma, P. Richard, X. Huang, L. Zhao, G. Chen, C. Matt, F. Bisti *et al.*, Nat. Phys. **11**, 724 (2015).
[28] L. Yang, Z. Liu, Y. Sun, H. Peng, H. Yang, T. Zhang, B. Zhou, Y. Zhang, Y. Guo, M. Rahn *et al.*, Nat. Phys. **11**, 728 (2015).
[29] Y. Sun, S.-C. Wu, and B. Yan, Phys. Rev. B **92**, 115428 (2015).
[30] S.-Y. Xu, N. Alidoust, I. Belopolski, Z. Yuan, G. Bian, T.-R. Chang, H. Zheng, V. N. Strocov, D. S. Sanchez, G. Chang *et al.*, Nat. Phys. **11**, 748 (2015).
[31] S.-Y. Xu, I. Belopolski, D. S. Sanchez, C. Zhang, G. Chang, C. Guo, G. Bian, Z. Yuan, H. Lu, T.-R. Chang *et al.*, Sci. Adv. **1**, e1501092 (2015).
[32] N. Xu, H. Weng, B. Lv, C. Matt, J. Park, F. Bisti, V. Strocov, E. Pomjakushina, K. Conder, N. Plumb *et al.*, Nat. Commun. **7**, 11006 (2016).
[33] Z. Liu, L. Yang, Y. Sun, T. Zhang, H. Peng, H. Yang, C. Chen, Y. Zhang, Y. Guo, D. Prabhakaran *et al.*, Nat. Mater. **15**, 27 (2016).
[34] D.-F. Xu, Y.-P. Du, Z. Wang, Y.-P. Li, X.-H. Niu, Q. Yao, P. Dudin, Z.-A. Xu, X.-G. Wan, and D.-L. Feng, Chin. Phys. Lett. **32**, 107101 (2015).
[35] D. Kim, S. Thomas, T. Grant, J. Botimer, Z. Fisk, and J. Xia, Sci. Rep. **3**, 3150 (2013).
[36] Z. Ren, A. A. Taskin, S. Sasaki, K. Segawa, and Y. Ando, Phys. Rev. B **82**, 241306(R) (2010).
[37] P. E. Blöchl, Phys. Rev. B **50**, 17953 (1994).
[38] G. Kresse and D. Joubert, Phys. Rev. B **59**, 1758 (1999).
[39] G. Kresse and J. Hafner, Phys. Rev. B **47**, 558 (1993).
[40] G. Kresse and J. Furthmüller, Comput. Mater. Sci. **6**, 15 (1996).
[41] G. Kresse and J. Furthmüller, Phys. Rev. B **54**, 11169 (1996).
[42] J. P. Perdew, A. Ruzsinszky, J. Tao, V. N. Staroverov, G. E. Scuseria, and G. I. Csonka, J. Chem. Phys. **123**, 062201 (2005).
[43] J. P. Perdew, K. Burke, and M. Ernzerhof, Phys. Rev. Lett. **77**, 3865 (1996).
[44] A. D. Becke and E. R. Johnson, J. Chem. Phys. **124**, 221101 (2006).
[45] F. Tran and P. Blaha, Phys. Rev. Lett. **102**, 226401 (2009).
[46] N. Marzari and D. Vanderbilt, Phys. Rev. B **56**, 12847 (1997).
[47] I. Souza, N. Marzari, and D. Vanderbilt, Phys. Rev. B **65**, 035109 (2001).
[48] W. Bensch and W. Heid, Acta Crystallogr. Sect. C **51**, 2205 (1995).
[49] S. Furuseth, K. Selte, and A. Kjekshus, Acta Chem. Scand. **19**, 7 (1965).
[50] R. Ling and C. Belin, C. R. Acad. Sci. Paris **292**, 891 (1981).
[51] A. A. Abrikosov and A. Beknazarov, *Fundamentals of the Theory of Metals* (North-Holland, Amsterdam, 1988).
[52] D. Shoenberg, *Magnetic Oscillations in Metals* (Cambridge University Press, Cambridge, 1984).
[53] S. Y. Zhou, T.-L. Xia *et al.* (unpublished).
[54] Y. Li, J. Wang, T. Wang, X. Xu, C. Xi, C. Cao, and J. Dai, arXiv:1601.02062.
[55] A. Kokalj, Comput. Mater. Sci. **28**, 155 (2003).